



HAL
open science

Experimental and theoretical investigation on interactions between xylose-containing hemicelluloses and procyanidins

Xuwei Liu, Jiayi Li, Agnès Rolland-Sabaté, Serge Perez, Carine Le Bourvellec, Catherine M.G.C. Renard

► To cite this version:

Xuwei Liu, Jiayi Li, Agnès Rolland-Sabaté, Serge Perez, Carine Le Bourvellec, et al.. Experimental and theoretical investigation on interactions between xylose-containing hemicelluloses and procyanidins. Carbohydrate Polymers, 2022, 281, pp.119086. 10.1016/j.carbpol.2021.119086 . hal-03532362

HAL Id: hal-03532362

<https://hal.inrae.fr/hal-03532362v1>

Submitted on 22 Jul 2024

HAL is a multi-disciplinary open access archive for the deposit and dissemination of scientific research documents, whether they are published or not. The documents may come from teaching and research institutions in France or abroad, or from public or private research centers.

L'archive ouverte pluridisciplinaire **HAL**, est destinée au dépôt et à la diffusion de documents scientifiques de niveau recherche, publiés ou non, émanant des établissements d'enseignement et de recherche français ou étrangers, des laboratoires publics ou privés.



Distributed under a Creative Commons Attribution - NonCommercial 4.0 International License

Experimental and theoretical investigation on interactions between xylose-containing hemicelluloses and procyanidins

Xuwei Liu^{a,b}, Jiayi Li^c, Agnès Rolland-Sabaté^b, Serge Perez^d, Carine Le Bourvellec^{b,*}, Catherine M.G.C. Renard^{b,e}

^aCollege of Food Science, South China Agricultural University, 483 Wushan Road, Guangzhou 510642, China

^bINRAE, Avignon University, UMR408 SQPOV, F-84000 Avignon, France

^cState Key Laboratory of Microbial Metabolism, Joint International Research Laboratory of Metabolic & Developmental Sciences, School of Life Sciences & Biotechnology, Shanghai Jiao Tong University, 200240 Shanghai, China

^dCNRS, CERMAV, University Grenoble Alpes, 38000 Grenoble, France

^eINRAE, TRANSFORM, F-44000 Nantes, France

Corresponding authors*

Carine Le Bourvellec (carine.le-bourvellec@inrae.fr)

INRAE, UMR408 SQPOV « Sécurité et Qualité des Produits d'Origine Végétale » 228 route de l'Aérodrome

CS 40509

F-84914 Avignon cedex 9

Tél: +33 (0)4 32 72 25 35

Fax: +33 (0)4 32 72 24 92

Others authors

Xuwei Liu: liuxwell@126.com; xuwei.liu@scau.edu.cn

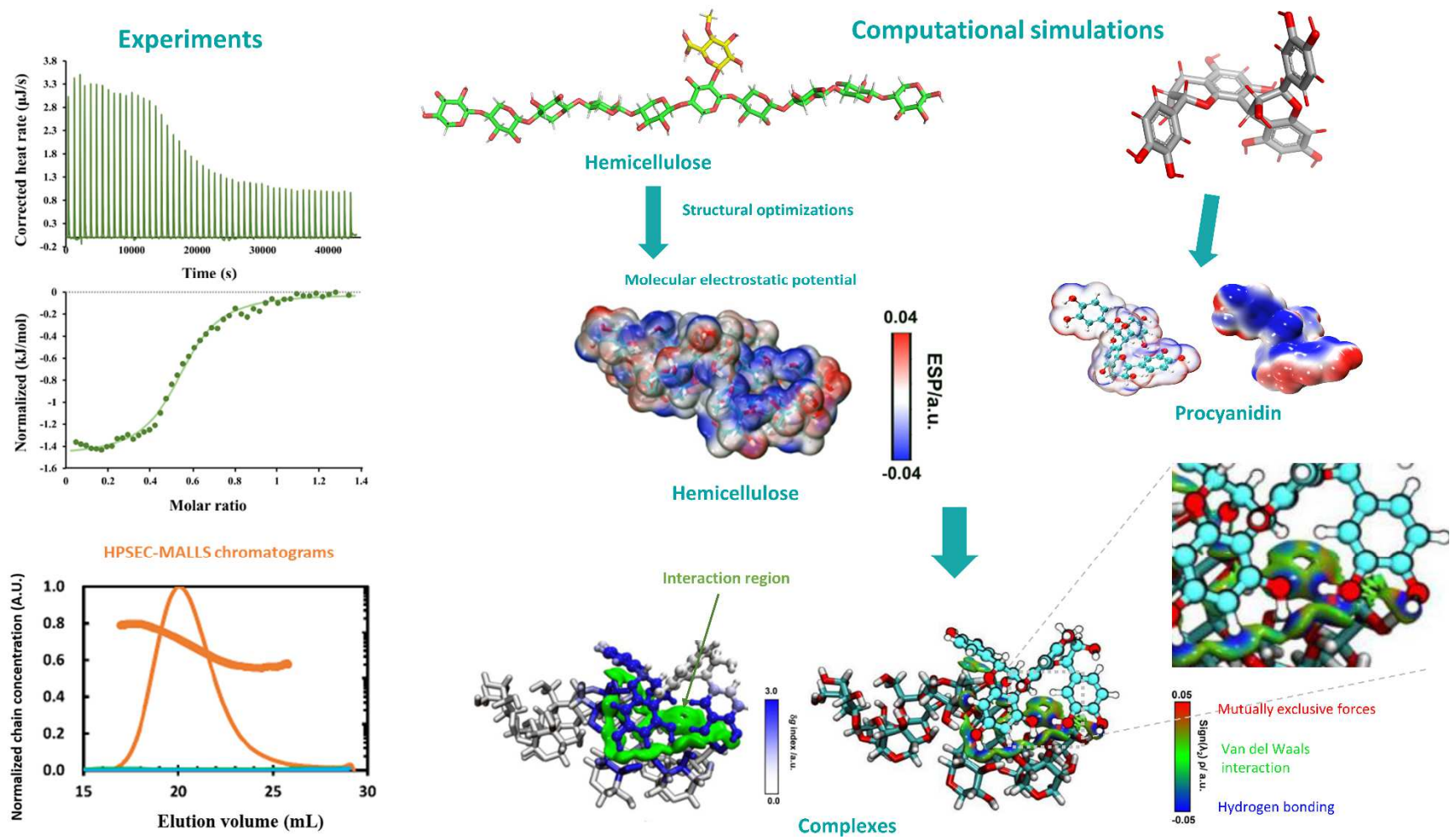
Jiayi Li: jemmylee@sjtu.edu.cn

Agnès Rolland-Sabaté: agnes.rolland-sabate@inrae.fr

Serge Perez: spsergeperez@gmail.com

Catherine M.G.C Renard: catherine.renard@inrae.fr

Graphical Abstract



1 **Abstract**

2 During processing of plant-based foods, cell wall polysaccharides and polyphenols,
3 such as procyanidins, interact extensively, thereby affecting their physicochemical
4 properties along with their potential health effects. Although hemicelluloses are
5 second only to pectins in affinity for procyanidins in cell walls, a detailed study of
6 their interactions lacks. We investigated the interactions between representative
7 xylose-containing water-soluble hemicelluloses and procyanidins. Turbidity, ITC and
8 DLS were used to determine the relative affinities, and theoretical calculations further
9 ascertained the interactions mechanisms. Xyloglucan and xylan exhibited respectively
10 the strongest and weakest interactions with procyanidins. The different arabinoxylans
11 interacted with procyanidins in a similar strength, intermediate between xyloglucans
12 and xylans. Therefore, the strength of the interaction depended on the structure itself
13 rather than on some incidental properties, e.g., viscosity and molar mass. The
14 arabinose side-chain of arabinoxylan did not inhibit interactions. The computational
15 investigation corroborated the experimental results in that the region of interaction
16 between xyloglucan and procyanidins was significantly wider than that of other
17 hemicelluloses.

18 **Keywords:** Condensed tannin; Polysaccharide; Xyloglucan; Noncovalent binding;
19 ITC; Molecular simulation

20 **Abbreviations:**

21 HPSEC-MALLS, High Performance Size-Exclusion Chromatography coupled with
22 Multi-Angle Laser Light Scattering; ITC, Isothermal Titration Calorimetry; DLS,
23 Dynamic Light Scattering; \overline{DP}_n , number average Degree of Polymerization; \overline{M}_w ,
24 weight-average molar mass; IGM, Independent Gradient Model; VMD, Visual
25 Molecular Dynamics.

26 **1. Introduction**

27 The polyphenols in fruits and vegetables display many potential biological
28 activities, and their dietary intake is related to a reduced risk of suffering from a
29 variety of chronic diseases (Koch, 2019). In addition to some endogenous factors,
30 such as microbiota and related digestive enzymes, food substrates (e.g., dietary fiber)
31 can also significantly regulate their bioavailability and further metabolism (Seal,
32 Courtin, Venema, & de Vries, 2021). In general, most of the ingested polyphenols,
33 especially the macromolecular polyphenols (e.g., procyanidins) are non-bioavailable
34 in the stomach and small intestine. These unabsorbed polyphenols can be transported
35 to the colon by dietary fiber, where bacteria may metabolize them as bioavailable
36 simple phenolic acids (Cui et al., 2019). This process may mediate the potential
37 beneficial effects of dietary fiber-polyphenol complexes, as they or their catabolites
38 may be absorbed and utilized by the human body (Jakobek & Matić, 2019; Le
39 Bourvellec et al., 2019). Therefore, the interactions between dietary fibers and
40 polyphenols may affect the bioavailability of polyphenols.

41 Among the dietary fibers, hemicelluloses have not benefited from significant
42 attention. They are heteropolysaccharides, such as xylan, arabinoxylan and
43 xyloglucan, including various sugar monomers. They have a moderate affinity with
44 polyphenols in cell walls. Hence, the affinity of procyanidins is greatest for pectins
45 followed by xyloglucan, and lowest for cellulose (Le Bourvellec, Bouchet, & Renard,
46 2005). In addition, by a step-wise removal of pectins and hemicelluloses in the grape
47 cell wall or apple cell wall, the binding capacity of proanthocyanidins to the

48 remaining cell walls is significantly reduced (Le Bourvellec, Watrelot, Ginies, Imberty,
49 & Renard, 2012; Ruiz-Garcia, Smith, & Bindon, 2014), but cell walls still have an
50 affinity for proanthocyanidins. However, Phan, Flanagan, D’Arcy, & Gidley (2017)
51 compared the selection of different cellulose-based composite materials (cellulose,
52 cellulose-xyloglucan, cellulose-arabinoxylan, cellulose-pectin) for the adsorption
53 capacity of polyphenols. They found that cellulose is the main binder, whereas
54 hemicelluloses (e.g., xyloglucan and arabinoxylan) do not contribute to the adsorption
55 of catechins (Phan et al., 2017). Therefore, the adsorption capacity of specific
56 polysaccharides to specific polyphenols differs. The knowledge of the nature of the
57 interaction occurring between different hemicelluloses and polyphenols still needs
58 clarification.

59 Polyphenols constitute a large group of plant compounds, mainly divided into
60 phenolic acids, flavonoids, stilbenes, and lignans. Procyanidins are the most abundant
61 macromolecular antioxidants in food and diet (Liu, Le Bourvellec, Guyot, & Renard,
62 2021; Saura-Calixto & Pérez-Jiménez, 2018). They are primarily composed of
63 (-)-epicatechin units. Their number average degree of polymerization (\overline{DP}_n) varies
64 significantly between species and cultivars. Generally, the ability of polysaccharides
65 to interact with procyanidins is directly proportional to their molecular weight, that is,
66 \overline{DP}_n (Liu, Le Bourvellec, & Renard, 2020; Renard, Watrelot, & Le Bourvellec, 2017).

67 While the interactions between pectins and procyanidins have been thoroughly
68 studied (Liu et al., 2020; Liu, Renard, Bureau, & Le Bourvellec, 2021; Liu, Renard,
69 Rolland-Sabaté, & Le Bourvellec, 2021; Watrelot, Le Bourvellec, Imberty, & Renard,

70 2014), the corresponding knowledge for hemicelluloses, which are the other main
71 non-cellulosic component in the cell walls, is limited. Notably, the relative binding
72 capacity of various hemicellulose components, along with affinity and binding
73 mechanism, remains to be resolved. Therefore, the present study aims to explore the
74 interaction mechanism occurring between hemicelluloses and procyanidins using a
75 combination of techniques including isothermal titration calorimetry (ITC), UV-Vis
76 spectroscopy, high performance size-exclusion chromatography coupled with
77 multi-angle laser light scattering (HPSEC-MALLS) and dynamic light scattering
78 (DLS). In complement, the reactive sites of procyanidins and different hemicelluloses,
79 where explored using the density functional theory (DFT) level, through electrostatic
80 potential (ESP) and frontier molecular orbital (FMO) analysis. Further conformational
81 analysis of intra and intermolecular interactions provided detailed insights about the
82 nature and the strength of the mechanism underlying the interactions between
83 procyanidins and hemicelluloses. The present study contributes to the understanding
84 of the effects of structure, molar mass, viscosity and side chains on interactions
85 through probing the binding of selected procyanidins to different types of
86 hemicellulose components: xylan, xyloglucan and five arabinoxylans. This set of
87 results provides a reference for further study on the effect of the whole plant cell wall
88 system on the bioavailability of procyanidins to better understand the underlying
89 implications of both human nutrition and health interactions.

90 **2. Materials and methods**

91 **2.1. Standards and Chemicals**

92 The standards of arabinose, mannose, glucose, fucose, xylose, rhamnose, and
93 galactose were obtained from Fluka (Buchs, Switzerland). Arabinoxylan (Wheat flour)
94 with low /medium/high viscosity, arabinoxylan with 30% and 22% arabinose content,
95 xyloglucan (Tamarind), and xylan (Beechwood) were purchased from Megazyme
96 (Bray, Ireland).

97 **2.2. Procyanidins preparation**

98 Procyanidins (DP9 and DP39) were prepared from two apple varieties ('Marie
99 Menard' and 'Avrolles'), respectively, as described in [Liu, Renard, Rolland-Sabaté, &
100 Le Bourvellec \(2021\)](#). Briefly, aqueous acetone fractions were collected after washing
101 by hexane and methanol, and then purified using a LiChrospher 100 RP-18 (12 µm,
102 Merck, Darmstadt, Germany) column and further characterized following the
103 principles described by [Guyot, Marnet, Sanoner, & Drilleau, \(2001\)](#). The procyanidins
104 contained about 800 mg/g of phenolic compounds, primarily procyanidins plus traces
105 of (-)-epicatechin, 5'-caffeoylquinic acid, *p*-coumaroylquinic acid, phloridzine, and
106 flavonols ([Supplementary Table 1](#)).

107 **2.3. Macromolecular characteristics of hemicelluloses**

108 Macromolecular features of initial (2.5 g/L) and free hemicelluloses were
109 detected by HPSEC-MALLS as described by [Liu, Renard, Rolland-Sabaté, Bureau, &
110 Le Bourvellec \(2021\)](#). Briefly, samples (100 µL) after being filtered were injected in a
111 Shimadzu series LC system including a diode array detector (DAD), a refractive
112 index detector (RID) (Shimadzu, Kyoto, Japan), and a MALLS (DAWN HELEOS 8+,
113 equipped with a K5 flow cell and a GaAs laser at $\lambda = 660$ nm) from Wyatt Technology

114 Co. (Santa Barbara, CA, USA). Hemicelluloses were separated on
115 PolySep-GFC-P3000, P5000 and P6000 300 × 7.8 mm columns (40 ° C) equipped
116 with a guard column from Phenomenex (Le Pecq, France) eluted by citrate/phosphate
117 buffer (0.1 M, pH 3.8) at 0.6 mL/min. Zimm fitting method with a one order
118 polynomial fit was used to calculate the weight-average molar mass (\bar{M}_w)
119 (Rolland-Sabaté, Colonna, Potocki-Véronèse, Monsan, & Planchot, 2004). A
120 refractive index increment (dn/dc) value of 0.146 mL/g was used to calculate the
121 concentration of hemicelluloses. Astra software® (version 7.1.4, Wyatt Technology
122 Co.) was used to calculate and analyze the results. Injections were carried out in
123 duplicates.

124 **2.4. Isothermal titration calorimetry**

125 The entropy and enthalpy changes of procyanidins binding to hemicelluloses
126 were measured in a citrate/phosphate buffer (0.1 M, pH 3.8) at 25 °C with stirring at
127 90 rev/min, using a TAM III isothermal microcalorimeter (TA instruments, New
128 Castle, USA) as described by Liu, Renard, Rolland-Sabaté, & Le Bourvellec (2021).
129 The hemicellulose samples (15 mM xylose equivalent, a similar concentration for
130 xyloglucan, ca. 3.75 g/L) were injected into an 850 µL sample cell of stainless steel
131 and equilibrated until the baseline was stable. Over 20 min time intervals, 50
132 injections of 5 µL procyanidins (30 mmol/L in (-)-epicatechin equivalent) were
133 titrated into the sample cell. The raw ITC data, measured as the heating power input
134 against time, were collected continuously and peak integration was fitted by TAM
135 assistant software (NanoAnalyze 3.10.0). The experiments were carried out in

136 duplicates.

137 **2.5. Phase diagram**

138 A spectrophotometric method was used to study hemicellulose-procyanidin
139 interactions as described by [Liu, Renard, Rolland-Sabaté, & Le Bourvellec \(2021\)](#).

140 The absorbance values were collected using a SAFAS flx-Xenius XM
141 spectrofluorimeter (SAFAS, Monaco) at 650 nm on a 96-well microplate. Each
142 experiment was performed in triplicate, and the data were recorded at 25 °C, in a
143 citrate/phosphate buffer (0.1 M, pH 3.8). A serial procyanidin solutions (0, 0.06, 0.12,
144 0.24, 0.46, 0.94, 1.875, 3.75, 7.5, 15, 30 and 60 mmol/L (-)-epicatechin equivalent)
145 and hemicellulose solutions (0, 0.03, 0.06, 0.117, 0.47, 1.875, 7.5 and 30 mmol/L
146 xylose equivalent, a similar concentration for xyloglucan) were prepared along the
147 lines and columns, respectively. Each procyanidin/hemicellulose mixture was
148 prepared by mixing a constant volume of procyanidin and hemicellulose solutions (50
149 µL). The mixture was stirred for 20 s before each measurement. After the test,
150 microplates were centrifuged 10 min at 2100×g. Free procyanidins and hemicelluloses
151 were collected in the supernatant and then analyzed by HPLC-DAD with
152 thioacidolysis and HPSEC-MALLS, respectively.

153 **2.6. Theoretical calculation method**

154 The initial structures of monosaccharides (rhamnose, arabinose, xylose, mannose,
155 glucose) and procyanidin B2 were download from PubChem Compound database
156 (<https://pubchem.ncbi.nlm.nih.gov/>). Five structure of hemicelluloses (AXHB:
157 arabinoxylan (38% Ara), AXMB: arabinoxylan (30% Ara), AXLB: Arabinoxylan (22%

158 Ara), Xyloglucan, Xylan were built using Polys-Glycan Builder (Pérez & Rivet, 2021)
159 and displayed using SweetUnitMol software (Pérez, Tubiana, Imbert, & Baaden,
160 2015). Structural optimizations were obtained at the B3LYP-D3/6-31+G** level.
161 Single-point energy calculations were performed on the optimized structures using a
162 larger basis set standard Pople style, 6-311+G(d,p) basis sets and SMD solvation
163 model correction. As for the five different hemicelluloses, PM7 method was applied
164 to optimize these initial geometries in a rough level, and Gaussian 16 (Frisch et al.,
165 2016) software was adopted to obtain the precise geometries at a level of B3LYP-D3
166 /6-31+G**.

167 Since conformational space increases rapidly with degrees of freedom in small
168 molecules, we conducted modeling studies of samples based on an efficient
169 conformer search algorithm developed by the Grimme group, which can provide
170 adequate sampling of the conformational space. Possible initial geometries were
171 generated using xtb software (Grimme, Bannwarth, & Shushkov, 2017). All the
172 lowest-energy conformations were obtained with the conformer rotamer ensemble
173 sampling tool (CREST) (Pracht, Bohle, & Grimme, 2020) and Molclus program (Lu
174 et al., 2020), respectively (See details in the Supporting Information). Then,
175 non-covalent interaction (NCI) analysis was carried out (additional notes in the
176 Supporting Information). Frontier Molecular Orbital (FMO) analysis (Huang et al.,
177 2020) and Electrostatic potential (ESP) analysis were finally performed by Multiwfn
178 3.7 software package (Lu & Chen, 2012).

179 **2.7. Statistical analysis**

180 All chemical analyses are expressed as mean values of analytical duplicates and
181 triplicates, and the reproducibility of the results is presented as pooled standard
182 deviations (Pooled SD) (Box, Hunter, & Hunter, 1978). Heatmap analyses were
183 performed using Python software (version 3.6) with Seaborn package (Waskom,
184 2014).

185 **3. Results and discussion**

186 **3.1. Characterization of hemicelluloses**

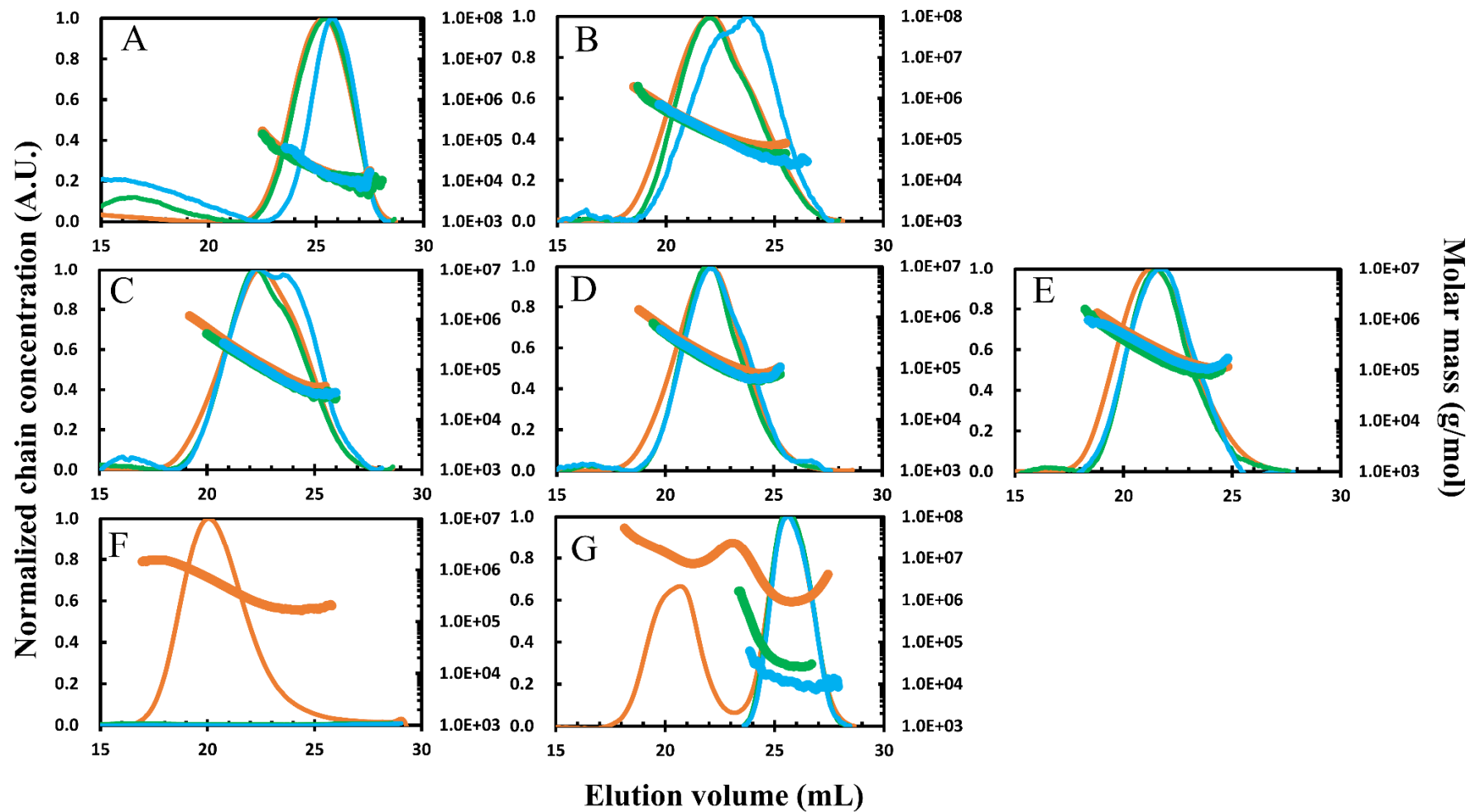
187 Table 1 lists the compositions and structures of the hemicelluloses, whereas
188 Figure 1 displays their molar mass and size distributions. Arabinoxylan (low viscosity)
189 (AXLV), arabinoxylan (medium viscosity) (AXMV) and arabinoxylan (high viscosity)
190 (AXHV) have similar sugar compositions, e.g., arabinose content (35 %), and their
191 molar mass increase with their viscosity (from 2.2 to 3.9 x 10⁵ g/mol). Moreover, to
192 compare the influence of the arabinose substitution on their interaction with
193 procyanidins, arabinoxylans with different arabinose contents were introduced, i.e.,
194 with 30% arabinose substituents (AXMB) and with 22% (AXLB): AXMB exhibited a
195 molar mass similar to AXMV whereas AXLV showed a ten times lower molar mass.
196 The addition of xyloglucan (XYLO) and xylan (XYLA) allowed the comparison of
197 the effect of xylose-containing hemicelluloses on procyanidin interactions. XYLO
198 exhibited the highest molar mass, while AXLB showed the lowest (Table 1). The
199 molar mass of xylan was not applicable due to possible interaction with the column.

200 **Table 1.** Neutral sugar compositions (mg/g dry weight) and weight-average molar mass ($\times 10^3$ g/mol) of hemicelluloses.

Samples	Rha	Fuc	Ara	Xyl	Man	Gal	Glc	Total	\overline{M}_w
AXLV	1	0	331	608	3	8	5	955	222
AXMV	1	0	335	636	2	6	3	984	261
AXHV	1	0	343	641	0	2	3	990	391
AXMB	1	0	288	693	0	7	5	995	257
AXLB	1	0	209	733	0	6	5	954	24
XYLO	1	0	12	282	140	0	399	834	774
XYLA	12	0	6	716	10	0	8	753	NA
<i>Pooled SD</i>	<i>0.7</i>	<i>0</i>	<i>3.3</i>	<i>17.2</i>	<i>1.1</i>	<i>0.4</i>	<i>5.3</i>	<i>23.1</i>	<i>19.6</i>

201 Rha: rhamnose, Fuc: fucose, Ara: arabinose, Xyl: xylose, Man: mannose, Gal: galactose, Glc: glucose. \overline{M}_w , weight-average molar mass. AXLV: Arabinoxylan (low
 202 viscosity); AXMV: Arabinoxylan (medium viscosity); AXHV: Arabinoxylan (high viscosity); AXMB: Arabinoxylan (30% Ara); AXLB: Arabinoxylan (22% Ara);
 203 XYLO: Xyloglucan; XYLA: Xylan. Pooled SD: pooled standard deviation. NA: Not applicable.

204






205

206

207

Fig. 1. HPSEC-MALLS chromatograms and molar mass vs elution volume for the hemicellulose samples. A, B, C, D, E, F and G: AXLB, AXMB, AXLV, AXMV, AXHV, XYLO and XYLA, respectively. —, — and —: normalized chain concentration of hemicelluloses before interaction, after interaction with DP9 and DP 39,

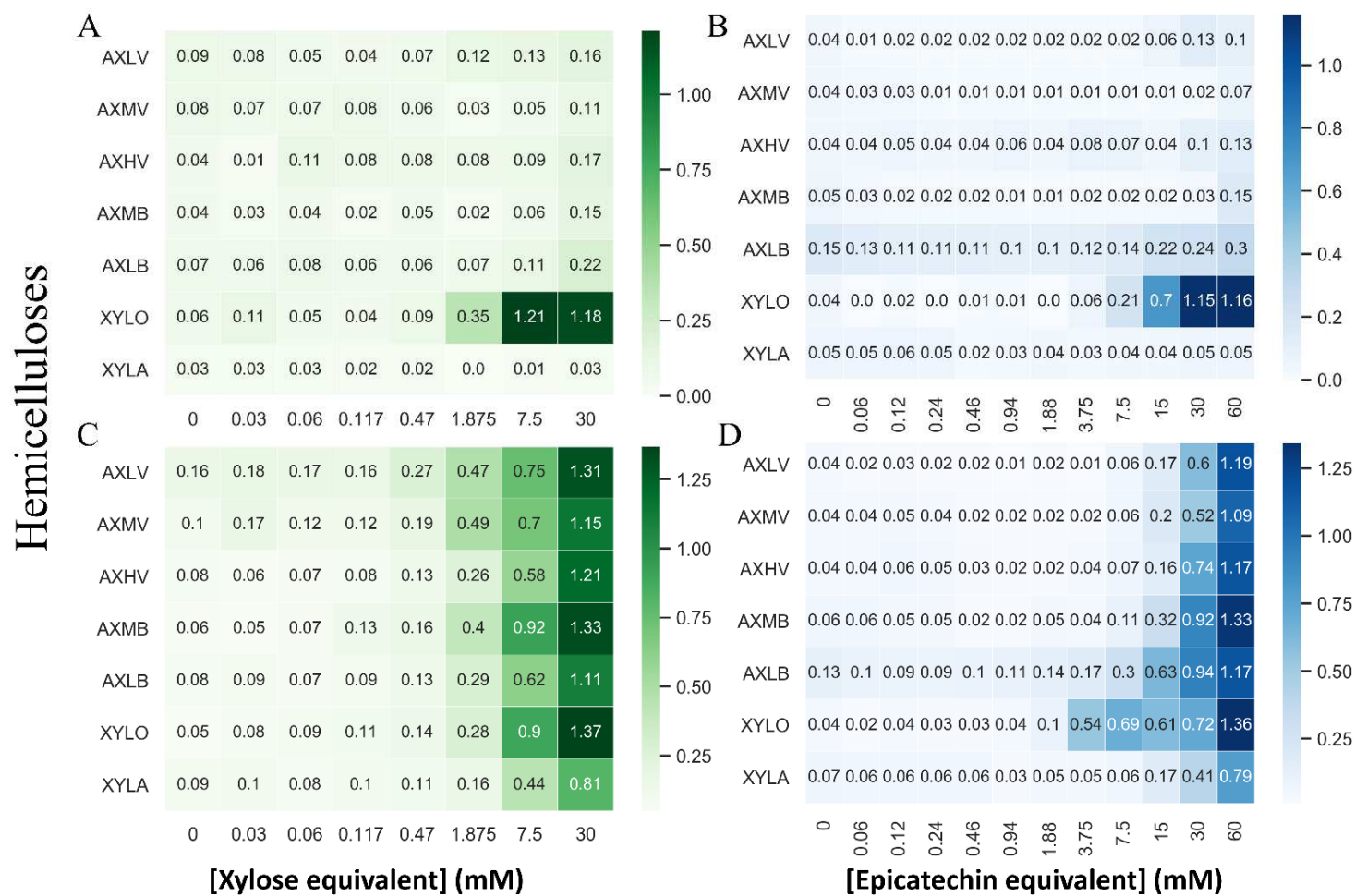
208 respectively; ,  and  : molar mass of hemicelluloses before interaction, after interaction with DP9 and DP 39. AXLB: Arabinoxylan (22% Ara); AXMB:
209 Arabinoxylan (30% Ara); AXLV: Arabinoxylan (low viscosity); AXMV: Arabinoxylan (medium viscosity); AXHV: Arabinoxylan (high viscosity); XYLO: Xyloglucan;
210 XYLA: Xylan.

211 **3.2. Phase diagram**

212 Turbidity analysis is an effective method for the direct detection of interactions;
213 the increase in turbidity is proportional to the number and size of the complexes
214 (WatreLOT, Le Bourvellec, Imberty, & Renard, 2013; WatreLOT et al., 2014). The
215 turbidity of the xyloglucan mixture containing procyanidin DP9 increased
216 significantly with increasing xyloglucan concentration (Fig. 2A). However, there was
217 minimal change for the hemicelluloses with a xylan backbone, with an increase only
218 at 30 mM xylose equivalents. Similarly, the absorbance of xyloglucan at the highest
219 concentration increased with increasing procyanidin DP9 concentration (Figure 2B),
220 while the hemicelluloses with a xylan backbone remained constant, which was
221 consistent with the trend in Fig. 2A. The overall aggregation capacity of
222 hemicelluloses (AXHV, AXMV, AXLV, AXMB, AXLB and xylan) with procyanidin
223 DP9 was lower than that of pectins, but the aggregation capacity of xyloglucan with
224 procyanidin DP9 was the same as that of kiwifruit pectins (Liu, Renard,
225 Rolland-Sabaté, & Le Bourvellec, 2021).

226 Interaction between hemicelluloses and procyanidin DP39 produced significantly
227 more aggregates than with DP9 (Fig. 2 C and D), the turbidity increased significantly
228 with increasing concentrations of either hemicellulose or procyanidin for all the
229 hemicelluloses tested, indicating a strong interaction with procyanidin DP39. The
230 addition of procyanidin DP39 also resulted in a significant increase in the particle
231 diameter of complexes determined by DLS (Supplementary Table 2). Procyanidin
232 DP39, rich in ortho phenolic groups and aryl rings, leads to a more extensive

233 aggregation of colloidal particles. The turbidity for hemicelluloses with procyanidins



234

235

236

Fig. 2. Heat map of the turbidity characteristics of interactions between hemicelluloses and procyanidins DP9/39. Absorbance at 650 nm, 25 °C, pH 3.8, 0.1 M, citrate/phosphate buffer. (A) and (C): Variation of absorbance of hemicelluloses at different concentrations (xylose equivalent, a similar concentration for xyloglucan) with

237 procyanidins DP9/39 (60 mM epicatechin equivalent). (B) and (D) Variation of absorbance of procyanidins DP9/39 (epicatechin equivalent) at different concentrations with
238 hemicelluloses (30 mM xylose equivalent, a similar concentration for xyloglucan: 7.5 g/L). AXLB: Arabinoxylan (22% Ara); AXMB: Arabinoxylan (30% Ara); AXLV:
239 Arabinoxylan (low viscosity); AXMV: Arabinoxylan (medium viscosity); AXHV: Arabinoxylan (high viscosity); XYLO: Xyloglucan; XYLA: Xylan. The experiments were
240 done in triplicates.

241

242 DP39 at 30 mM xylose equivalent (a similar concentration for xyloglucan: 7.5 g/L) or
243 60 mM (-)-epicatechin equivalent increased in the following order: Xylan < AXLB
244 \approx AXMV \approx AXHV \approx AXLV < AXMB < Xyloglucan. Therefore, xyloglucan
245 had the strongest aggregation capacity with procyanidins, followed by arabinoxylan
246 and xylan had the weakest aggregation capacity. The different types of arabinoxylans
247 had similar capacities. This result was consistent with the results of DLS
248 (Supplementary Table 2): the size of xylan increased the least, while xyloglucan
249 cannot be measured, because it directly produced obvious flocculent precipitation
250 with procyanidins. The viscosity and molar mass of hemicellulose were not the main
251 determinants (medium impact) of the strength of the interactions, a result that was
252 consistent with pectins (Liu, Renard, Rolland-Sabaté, & Le Bourvellec, 2021).
253 However, the arabinose sidechain of arabinoxylan did not inhibit the interactions. This
254 observation contrasted with the inhibition of interaction with procyanidins observed
255 for the pectin sidechains. The length of arabinoxylan sidechain composed of only one
256 monosaccharide may be not sufficient to cause spatial site blocking, while it does
257 contribute to decrease rigidity of the backbone.

258 **3.3. Characterization of unbound hemicelluloses and procyanidins**

259 The changes in free hemicelluloses and procyanidins after interaction were
260 explored using supernatants collected after turbidity measurements. After mixing of
261 the two participants (60 mM epicatechin equivalent for procyanidins and 30 mM
262 xylose equivalent for hemicelluloses, a similar concentration for xyloglucan: 7.5 g/L),
263 most of the hemicellulose-procyanidin complexes precipitated, and only a small

264 amount remained in the supernatant. \overline{M}_w values of free hemicelluloses and \overline{DP}_n of
265 free procyanidins exhibited a drastic decrease after interactions (Table 2). This
266 indicated that procyanidin DP9/39 were highly selective for the high molar mass
267 fractions of hemicellulose, especially for xyloglucan. Similarly, hemicelluloses were
268 highly selective for higher \overline{DP}_n of procyanidins, that is, DP39. Moreover,
269 xyloglucan was barely detectable in the supernatant of the DP39-xyloglucan complex
270 solution.

271 Fig. 1 shows the HPSEC-MALLS chromatograms of hemicelluloses that did not
272 form aggregates with procyanidins after interaction. The main peaks of free AXLB
273 and AXMB after interaction with procyanidin DP9 were not significantly different
274 from originals, while after interaction with procyanidin DP39, these main peaks were
275 slightly shifted to higher elution volumes indicating a lower molecular size. The main
276 peaks of free AXLV, AXMV and AXHV similarly shifted to higher elution volumes
277 after interaction with procyanidin DP9 and DP39. Whatever the procyanidins' DP,
278 xyloglucan was barely detectable in the supernatant after interaction, which indicated
279 that procyanidins interacted strongly with it. Finally, xylan lost its first main peak
280 after interaction indicating that procyanidins associated selectively with higher size
281 fraction of xylan (Fig. 1G). Therefore, large-sized hemicelluloses and highly
282 polymerized procyanidins were preferentially aggregated.

283 **Table 2.** Changes in molar mass of hemicelluloses and in the degree of polymerization of procyanidins before and after interactions between xylose-containing
 284 hemicelluloses and procyanidins DP9/39.

Sample	Initial hemicelluloses	Unbound hemicelluloses	Unbound PCA DP9	Unbound hemicelluloses	Unbound PCA DP39 with
	\bar{M}_w *	with PCA DP9	with hemicelluloses	with PCA DP39	hemicelluloses
	($\times 10^3$ g/mol)	\bar{M}_w	\overline{DP}_n of free PCA	\bar{M}_w	\overline{DP}_n of free PCA
		($\times 10^3$ g·mol ⁻¹)		($\times 10^3$ g·mol ⁻¹)	
AXLV	222	130 (-92 ^a)	8 (-1 ^b)	125 (-97 ^a)	25 (-14 ^b)
AXMV	261	175 (-86)	7 (-2)	162 (-99)	20 (-19)
AXHV	391	244 (-147)	7 (-2)	238 (-159)	18 (-21)
AXMB	257	182 (-75)	6 (-3)	118 (-139)	17 (-22)
AXLB	24	20 (-4)	7 (-2)	16 (-8)	19 (-20)
XYLO	774	NA	6 (-3)	NA	16 (-23)
XYLA	NA	NA	8 (-1)	NA	19 (-20)
<i>Pooled SD</i>	<i>19.6</i>	<i>5.3</i>	<i>0.5</i>	<i>3.4</i>	<i>1.2</i>

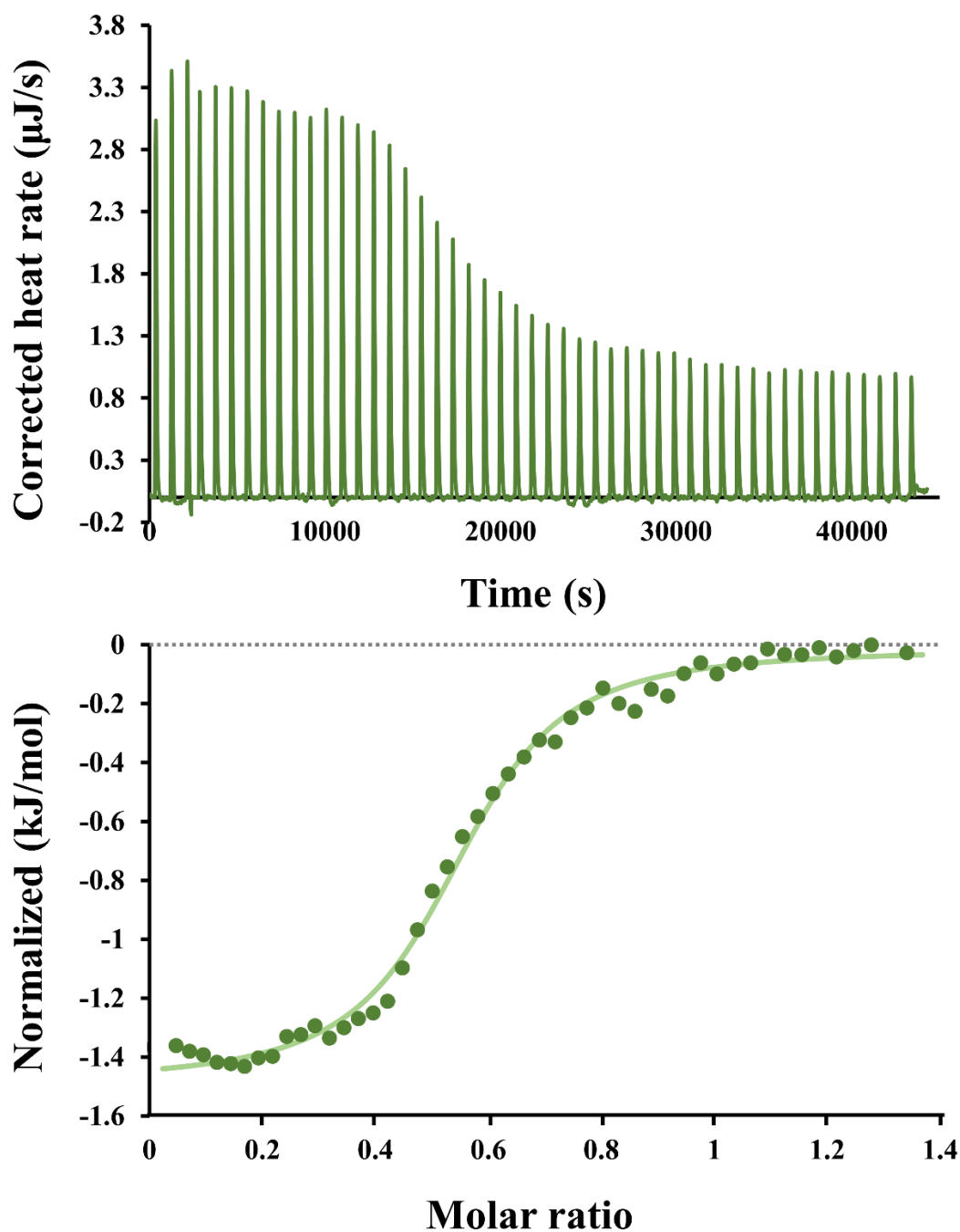
285 *data adapted from Table 1. Average of duplicates for each. \bar{M}_w : weight-average molar mass. \overline{DP}_n : number-average degree of polymerization. NA: Not applicable. ^a $\Delta \bar{M}_w$:
 286 difference of molar mass between hemicellulose unbound to procyanidin solutions after interaction with procyanidins and initial hemicelluloses in buffer. ^b $\Delta \overline{DP}_n$: difference
 287 of degree of polymerization between procyanidins unbound to hemicelluloses after interaction with hemicelluloses and initial procyanidins in buffer.
 288

289 3.4. Isothermal Titration Calorimetry (ITC)

290 ITC provides access to stoichiometric ratios and thermodynamic parameters, e.g.,
291 entropy and enthalpy changes, free energy and binding constants during the
292 interactions (Callies & Hernández Daranas, 2016; Liu et al., 2020). This method
293 provides detailed information which complements those derived from turbidity in the
294 detection of interactions. The titration of different hemicelluloses (7.5 and/or 15 mM
295 xylose equivalent, a similar concentration for xyloglucan, ca. 3.75/7.5 g/L) by
296 procyanidin DP9 (30 mM) led to endothermic peaks, but no curve and no titration
297 could be observed (data not shown). Therefore, no interaction could be measured for
298 the procyanidin DP9 using ITC.

299 Typical thermograms of titration of AXLV, AXMV, AXHV, AXMB, AXLB and
300 xylan (15 mM xylose equivalent, a similar concentration for xyloglucan, ca. 3.75 g/L)
301 titrated by procyanidin DP39 (30 mM (-)-epicatechin equivalent) showed strong
302 exothermic peaks. Blank experiments (procyanidin DP39 injection in buffer)
303 produced only small endothermic peaks, which were subtracted before integration
304 (Supplementary Fig. 1). These ITC titration curves are consistent with previous
305 studies on pectins (Fernandes et al., 2020; Liu, Renard, Rolland-Sabaté, & Le
306 Bourvellec, 2021; Watrelot et al., 2014). However, xyloglucan behaved very
307 differently from arabinoxylan and xylan upon mixing with procyanidin DP39 solution
308 (Fig. 3). The curve was similar to the typical curve of protein-ligand interactions
309 (Poncet-Legrand, Gautier, Cheynier, & Imberty, 2007), with a relatively sharply
310 reduced exothermic peak upon addition of procyanidins. As the concentration of

311 procyanidin increased, the number of available binding sites on xyloglucan decreased
312 until saturation, and the addition of more procyanidin led to a plateau. The mechanism
313 of their interaction may consist of three consecutive stages corresponding to (i) the
314 presence of very few particles, (ii) the formation of xyloglucan-procyanidin
315 aggregates of relatively small size, and (iii) the formation of precipitation upon further
316 addition of procyanidins.



317

318 **Fig. 3.** Thermogram of titration of xyloglucan with procyanidins DP39. The measurement of heat
 319 release at the top, while the molar enthalpy changes against (-)-epicatechin/xylose equivalent ratio after
 320 peak integration at the bottom.

321

322

323 **Table 3.** Thermodynamic parameters of interactions measured by ITC: hemicelluloses (15 mM xylose
 324 equivalent, 7.5 mM for xyloglucan) and procyanidins DP39 (30 mM (-)-epicatechin equivalent).

DP39	n	Ka (M ⁻¹)	Δ H (kJ/mol)	Δ S (J/mol/K)	Δ G (kJ/mol)	-TΔS (kJ/mol)	Enthalpy (%)	Entropy (%)
AXLV	0.094	5849	-0.31	71.09	-21.50	-21.20	1%	99%

AXMV	0.010	5472	-2.26	63.99	-21.34	-19.08	11%	89%
AXHV	0.089	4509	-0.34	68.81	-20.86	-20.52	2%	98%
AXMB	0.108	4600	-0.22	69.39	-20.90	-20.69	1%	99%
AXLB	0.010	424	-13.65	4.52	-14.99	-1.35	91%	9%
XYLO	0.554	7949	-1.47	69.73	-22.26	-20.79	7%	93%
XYLA	0.107	1452	-0.69	58.19	-18.04	-17.35	4%	96%
<i>Pooled</i>								
<i>SD</i>	0.002	144	0.54	0.85	0.77	0.86	-	-

325 Pooled SD: pooled standard deviation. n: stoichiometry, K_a : affinity level, ΔH , ΔS and ΔG : enthalpy,
 326 entropy and free enthalpy, respectively. T: temperature. AXLV: Arabinoxylan (low viscosity); AXMV:
 327 Arabinoxylan (medium viscosity); AXHV: Arabinoxylan (high viscosity); AXMB: Arabinoxylan (30%
 328 Ara); AXLB: Arabinoxylan (22% Ara); XYLO: Xyloglucan; XYLA: Xylan. Enthalpy (%) = $\Delta H / (\Delta H -$
 329 $T\Delta S) \times 100\%$; Entropy (%) = $-T\Delta S / (\Delta H - T\Delta S) \times 100\%$. Average of duplicates for each.

330

331

332 Stoichiometry (defined as ratio of (-)-epicatechin/xylose) was c.a. 0.1 for AXLV,
 333 AXHV, AXMB and xylan (1 molecule of (-)-epicatechin bound 10 molecules of
 334 xylose) and c.a. 0.6 for xyloglucan (1 molecule of (-)-epicatechin bound 2 molecules
 335 of xylose) using a one-site model. The association constant ranged between 424 M^{-1}
 336 and 7949 M^{-1} and increased in the sequence below: AXLB < Xylan < AXHV \approx
 337 AXMB \approx AXMV \approx AXLV < Xyloglucan (Table 3). The affinity range of
 338 hemicelluloses binding to procyanidins is between that of whole cell walls ($10^2/10^3$
 339 M^{-1}) and pectins ($10^3/10^4 M^{-1}$) (Brahem, Renard, Bureau, Watrelot, & Le Bourvellec,
 340 2019; Fernandes et al., 2020; Liu et al., 2020; Liu, Renard, Rolland-Sabaté, & Le
 341 Bourvellec, 2021). The association constants for strong affinity are generally larger
 342 than $10^4 M^{-1}$ (Turnbull & Daranas, 2003). Xyloglucan with a glucose backbone and
 343 xylose side-chains structure, and the highest molar mass, had the highest affinity for
 344 procyanidin DP39, indicating that glucose backbone facilitated the interaction with
 345 procyanidins. AXLB and xylan with the least arabinose and lower molar mass had
 346 lowest affinity for procyanidin DP39. For the other arabinoxylans, although they had

347 different sugar ratios, molar mass and viscosities, their affinities with procyanidins
348 were very close.

349 The strong entropy contribution ($-T\Delta S$ from -21 to -17 kJ/mol) showed that the
350 interactions between hemicelluloses (except for AXLB) and procyanidins were
351 mostly driven by entropy, i.e., by hydrophobic interactions and the release of water
352 molecules (Liu, Renard, Rolland-Sabaté, & Le Bourvellec, 2021; Poncet-Legrand et
353 al., 2007). The enthalpy contributions were higher for AXLB (ΔH : -14 kJ/mol)
354 indicating that interactions mostly involved hydrogen bonds. The entropy contribution
355 for AXLB was significantly lower than that of other hemicelluloses, which could
356 indicate that the hydrophobic interaction was more significant for their affinity with
357 procyanidins. Generally, pectin has a high affinity for procyanidins, which also due to
358 hydrophobic interaction forces (Liu, Renard, Rolland-Sabaté, & Le Bourvellec, 2021).
359 Therefore, of xylose-containing hemicelluloses, xyloglucan have highest affinity for
360 procyanidins. All other affinities were lower for hemicelluloses with a xylan backbone,
361 especially when the ramification by arabinose was limited. This observation
362 confirmed the results derived from the turbidity experiment. These two methods are
363 complementary, allowing higher sensitivity for detection of the interactions (haze
364 formation) on the one hand and access to stoichiometric ratio and binding enthalpy
365 (ITC) on the other hand. Turbidity measurements provide information on the
366 formation of insoluble complexes, but they can not provide information on the
367 mechanism and binding sites.

368 Furthermore, Phan et al. (2017) found that small polyphenol molecules (e.g.,

369 catechins and ferulic acid) selectively bind to the relatively hydrophobic and rigid
370 cellulose, rather than to the more hydrophilic and flexible arabinoxylan or xyloglucan.
371 This highlighted the role of polyphenol structure, that is, hemicelluloses may
372 preferentially bind macromolecular procyanidins, because procyanidins can provide
373 more hydroxyl groups and hydrophobic sites (Liu et al., 2020; Liu, Renard,
374 Rolland-Sabaté, & Le Bourvellec, 2021).

375 **3.5. Theoretical calculation of the interactions**

376 **3.5.1. Reactivity of monosaccharides**

377 Theoretical calculations revealed a mechanism that goes beyond the widely
378 accepted frontier molecular orbital (FMO) theory, which stated that the frontier
379 orbitals, that is, the highest occupied molecular orbital (HOMO) and the lowest
380 unoccupied molecular orbital (LUMO), were mainly responsible for chemical
381 reactivity (Huang et al., 2020). The smaller HOMO-LUMO gap defined the high
382 chemical reactivity and polarizability of compounds. Among the different
383 monosaccharide structural units, glucose and mannose had the relatively lower
384 HOMO-LUMO gap of 8.10 eV and 8.28 eV, respectively (Supplementary Fig. 2).
385 Compared with a higher HOMO-LUMO gap of 8.52 eV and 8.53 eV in xylose and
386 rhamnose, respectively, glucose and mannose units had the higher chemical reactivity
387 and could more easily interact with other molecules. Xyloglucan contains the highest
388 proportion of glucose. However, the content of xylose in xylan was the highest, and
389 the chemical properties of xylose and rhamnose are relatively inactive, making it
390 difficult for xylan to combine with other molecules to form a complex. For AXLB,

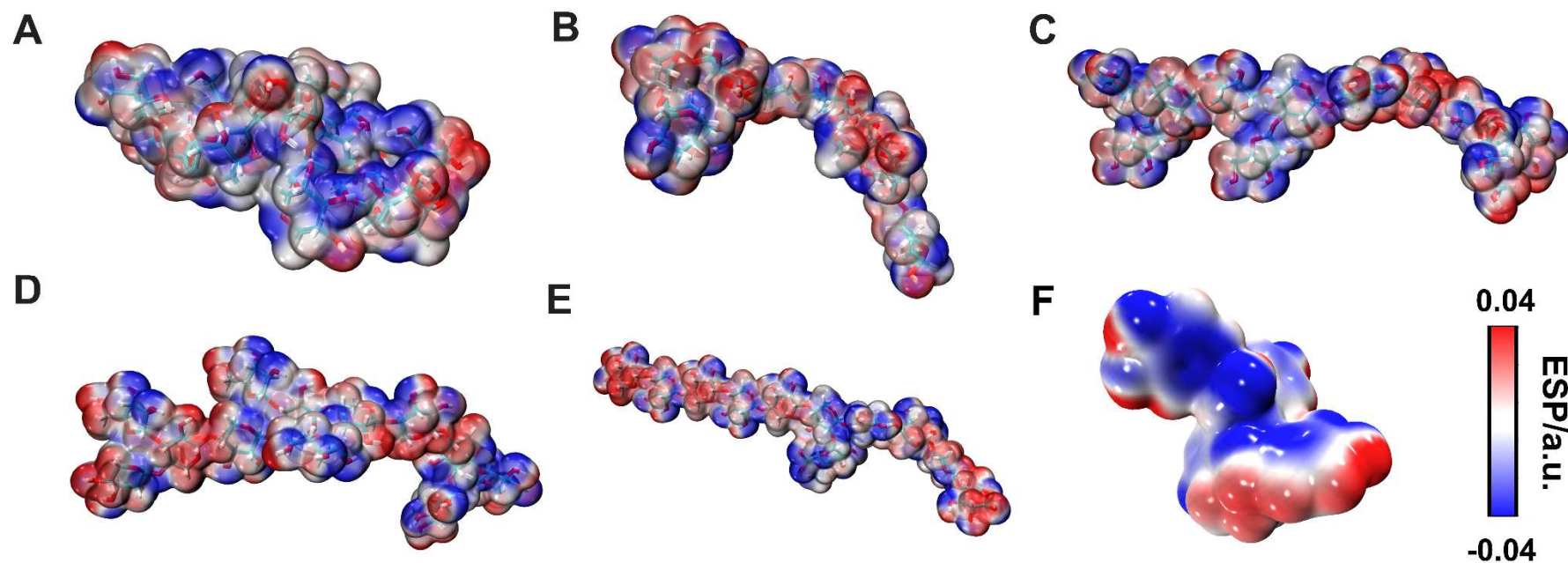
391 AXMB, and AXHB, the structure had a certain regularity: the content of arabinose
392 side-chains gradually increased, while the content of xylose (backbone) gradually
393 decreased. The higher content of xylose, which has less polarizability than the other
394 sugar monomers, explains the lower reactivity of AXLB. However, the reactivity of
395 the atoms on the monosaccharide structure is only one among other factor, and the
396 appropriate relative conformation of hemicelluloses and procyanidins remains the
397 dominant factor that drive the interactions. The backbone of xyloglucan and
398 xylan/arabinoxylan are the glucose and xylose backbone, respectively. In addition,
399 xylans are highly ordered, while arabinoxylans are less ordered and their arabinose
400 substituents influence the degree of rigidity of the structure (Selig, Thygesen, Felby,
401 & Master, 2015; Shrestha et al., 2019).

402 **3.5.2. Structured hemicelluloses**

403 Considering the large number of unit structures and the excessive number of atoms in
404 polymerized procyanidins, it is not possible at current stage for computers to modelize
405 these structures. Therefore, procyanidin B2 was used to model the local interaction
406 between hemicelluloses and procyanidins. The simulation of local interactions is an
407 important guide to subsequent global simulations. The molecular electrostatic
408 potential (ESP) on the molecular van der Waals (vdW) surfaces was calculated and
409 mapped for the five different xylose-containing hemicelluloses and procyanidin B2, in
410 order to gain further understanding of the molecular recognition behavior (Fig. 4).
411 The ESP on the van der Waals surface is appropriate to gather information about the
412 reaction site, molecular property, which is critical for studying and predicting

413 intermolecular interaction (Murray & Politzer, 2011). The pyran ring skeleton (PRS)
414 and CH₂OH group outside the ring presented quite different electrostatic potential
415 characters for different types of hemicellulose. The ESP value over the PRS carbons
416 was moderately negative. As for non-PRS part, that is, CH₂OH group, lone pair of
417 each oxygen atom leads to one or more ESP minima on the vdW surface. Each surface
418 maximum in the non-PRS part corresponds to a hydrogen atom. In addition, the
419 structural optimization of xyloglucan yields the formation of clusters, while
420 hemicelluloses with a xylan backbone still maintain long-chain extension.

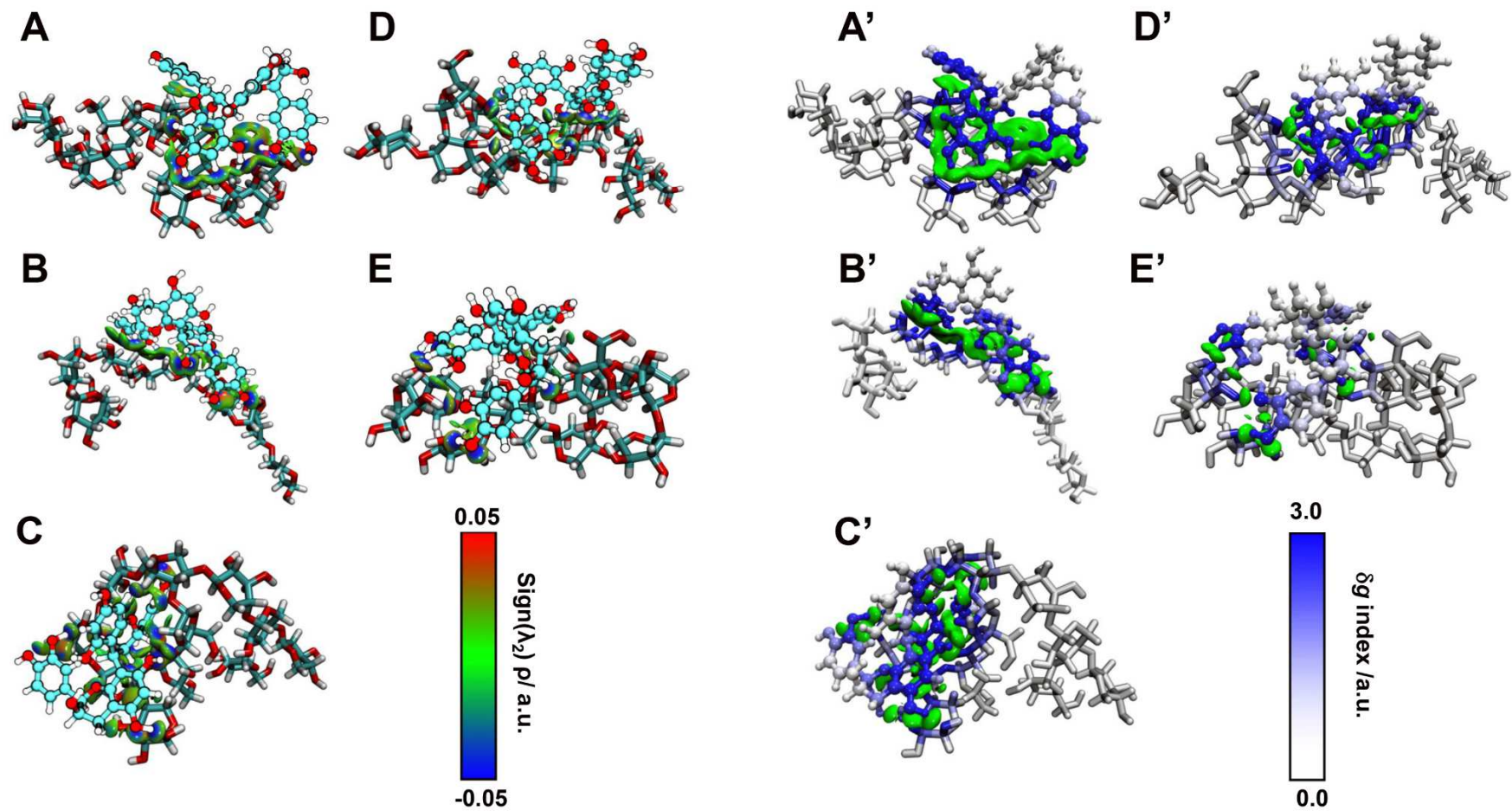
421 Lowest-energy conformer after conformation search were kept for further
422 calculations. The optimized binding geometry was meaningful since molecules
423 interact in a complementary manner of the electrostatic potential ESP to form
424 intermolecular interaction. The overall interaction energies in aqueous solution were
425 estimated to be -480, -319, -315, -306 and -246 kJ/mol and -274, -201, -193, -187 and
426 -160 kJ/mol before and after the counterpoise correction, in the cases of procyanidin
427 B2-Xyloglucan, procyanidin B2-AXLB, procyanidin B2-AXMB, procyanidin
428 B2-AXHB and procyanidin B2-Xylan, respectively.



429

430 **Fig. 4.** Molecular electrostatic potential maps. The optimized geometry of the five different hemicellulose compounds at the B3LYP-D3/6-31G(d,p)/SMD (water) level of
 431 theory and the molecular electrostatic potential (ESP) analysis results on 0.001 a.u. contours of the electronic density. (A): Xyloglucan, (B): AXLB (22% Ara), (C): AXMB
 432 (30% Ara), (D): AXHB (38% Ara), (E): Xylan, (F): Procyanidin B2, respectively. (Blue: negative regions; Red: positive regions). The color scale is also given in a.u.. AXLB:
 433 Arabinoxylan (22% Ara); AXMB: Arabinoxylan (30% Ara); AXHB: Arabinoxylan (38% Ara).

434



435
436
437

Fig. 5. Intermolecular interactions (isosurfaces: 0.05 a.u.) using Independent Gradient Model (IGM) analysis. The non-covalent interaction existed in procyanidin B2 and different hemicellulose compounds. Procyanidin B2-Xyloglucan (A), procyanidin B2-AXLB (B), procyanidin B2-AXMB (C), procyanidin B2-AXHB (D) and

438 procyanidin B2-xylan (E). Blue color represented hydrogen bonding interaction, and green represented van der Waals interaction. All isosurfaces are colored
439 according to a BGR (blue-green-red) scheme over the electron density range $-0.05 < \text{sign}(\lambda^2) \rho < 0.05$ a.u. Molecular structures were also colored based on atom g
440 indices using IGM analysis for procyanidin B2-Xyloglucan (A'), procyanidin B2-AXLB (B'), procyanidin B2-AXMB (C'), procyanidin B2-AXHB (D') and
441 procyanidin B2-xylan (E') colored according to their contributions to the binding. The relative importance of various atoms in inter-fragment interactions is
442 demonstrated by color intensity. White indicates no contribution to the complexation, and atoms in brighter blue contribute more strongly to the interactions. The
443 green ovals indicate the presence of interactions. AXLB: Arabinoxylan (22% Ara); AXMB: Arabinoxylan (30% Ara); AXHB: Arabinoxylan (38% Ara).

444 Independent gradient model (IGM) analysis revealed the existence of extensive
445 non-covalent interaction occurring between the procyanidin B2 and hemicelluloses.
446 The interactions occur through weak hydrogen bonds (light-blue area in isosurfaces)
447 and van der Waals interactions (green area in isosurfaces). It indicated the vital role of
448 non-covalent contacts facilitating the effective accommodation of target
449 hemicelluloses (Fig. 5). A π -stacking interaction complements the interactions
450 occurring between the aromatic ring of procyanidin B2 and hemicellulose. The main
451 contributions to these complexations occur between procyanidin B2 and
452 hemicelluloses (as schematically enlighten by the colouring of the atoms according to
453 their contribution to the complexation - see Fig. 4). The relative importance of various
454 atoms in inter-fragmentary interaction was demonstrated by using colors, with the
455 atoms in brighter red contributing more strongly to the interactions. In Fig. 4, the
456 volume of the interacting regions could be taken as an indication of the extent of
457 interaction. As a result, procyanidin B2 formed more and less extensive interaction
458 with xyloglucan and xylan residues, respectively, while other hemicelluloses were in
459 the middle. This observation was consistent with the results of the experimental study
460 conducted above. The simulations by Shrestha et al. (2019) showed that the
461 intermolecular interaction with cellulose was not influenced by arabinose side-chain
462 in arabinoxylan.

463 **4. Conclusions**

464 The present study evaluated the nature of the interactions between
465 xylose-containing hemicelluloses, having either a xylan or a glucan backbone, and

466 procyanidins by experimental and theoretical methods. Across all methods used, a
467 consistent ranking of the capacity of association with procyanidins emerges as
468 xyloglucan > arabinoxylans > xylan. Hemicelluloses preferentially associate with the
469 high polymerized procyanidin DP39. The various processing-structure-interaction of
470 hemicelluloses and procyanidins could tailor the functional properties of plant-derived
471 products and provide a practical guide to the retention and changes in polyphenols
472 during processing.

473 **Acknowledgements**

474 LIU Xuwei would like to acknowledge China Scholarship Council (CSC) and
475 Institut National de Recherche pour l'Agriculture, l'Alimentation, et l'Environnement
476 (INRAE) for financial support to his PhD study. The authors thank the TERSYS
477 Federative Research Structure (Platform 3A project, CPER 2014-2020) for the
478 support to the HPSEC-MALLS measures as well as the related financial support from
479 the French government, the department of Vaucluse, Avignon University, PACA
480 region, European funds for regional development and CNRS.

481 **Conflicts of interest**

482 The authors declare no conflicts of interest.

483 **CRedit authorship contribution statement**

484 **Xuwei Liu:** Investigation, Software, Formal analysis, Data curation, Writing - original
485 draft. **Jiayi Li:** Software, Formal analysis, Visualization, Writing - review & editing.

486 **Catherine M. G. C. Renard:** Conceptualization, Funding acquisition, Project

487 administration, Validation, Writing - review & editing. **Agnès Rolland-Sabaté:**
488 Supervision, Methods, Software, Formal analysis, Validation, Writing - review &
489 editing. **Serge Perez:** Software, Writing - review & editing. **Carine Le Bourvellec:**
490 Conceptualization, Funding acquisition, Supervision, Validation, Writing - review &
491 editing.

492 **References**

- 493 Brahem, M., Renard, C. M. G. C., Bureau, S., Watrelot, A. A., & Le Bourvellec, C.
494 (2019). Pear ripeness and tissue type impact procyanidin-cell wall interactions.
495 *Food Chemistry*, 275, 754–762. <https://doi.org/10.1016/j.foodchem.2018.09.156>
- 496 Callies, O., & Hernández Daranas, A. (2016). Application of isothermal titration
497 calorimetry as a tool to study natural product interactions. *Natural Product*
498 *Reports*, 33(7), 881–904. <https://doi.org/10.1039/c5np00094g>
- 499 Cui, J., Lian, Y., Zhao, C., Du, H., Han, Y., Gao, W., ... Zheng, J. (2019). Dietary
500 Fibers from Fruits and Vegetables and Their Health Benefits via Modulation of
501 Gut Microbiota. *Comprehensive Reviews in Food Science and Food Safety*, 18(5),
502 1514–1532. <https://doi.org/10.1111/1541-4337.12489>
- 503 Fernandes, P. A. R., Le Bourvellec, C., Renard, C. M. G. C., Wessel, D. F., Cardoso,
504 S. M., & Coimbra, M. A. (2020). Interactions of arabinan-rich pectic
505 polysaccharides with polyphenols. *Carbohydrate Polymers*, 230, 115–644.
506 <https://doi.org/10.1016/j.carbpol.2019.115644>
- 507 Frisch, M. J., Trucks, G. W., Schlegel, H. B., Scuseria, G. E., Robb, M. A.,
508 Cheeseman, J. R., ... others. (2016). Gaussian 16, Revision A. 03, Gaussian, Inc.,
509 Wallingford CT. *City*.
- 510 Grimme, S., Bannwarth, C., & Shushkov, P. (2017). A Robust and Accurate
511 Tight-Binding Quantum Chemical Method for Structures, Vibrational
512 Frequencies, and Noncovalent Interactions of Large Molecular Systems
513 Parametrized for All spd-Block Elements ($Z = 1-86$). *Journal of Chemical*
514 *Theory and Computation*, 13(5), 1989–2009.
515 <https://doi.org/10.1021/acs.jctc.7b00118>
- 516 Guyot, S., Marnet, N., Sanoner, P., & Drilleau, J.-F. (2001). Direct thiolysis on crude
517 apple materials for high-performance liquid chromatography characterization
518 and quantification of polyphenols in cider apple tissues and juices. In L. Packer
519 (Ed.), *Methods in Enzymology* (pp. 57–70). Elsevier Inc.
520 [https://doi.org/10.1016/S0076-6879\(01\)35231-X](https://doi.org/10.1016/S0076-6879(01)35231-X)

521 Huang, Q., Li, J., Shi, T., Liang, J., Wang, Z., Bai, L., ... Zhao, Y. L. (2020). Defense
522 Mechanism of Phosphorothioated DNA under Peroxynitrite-Mediated Oxidative
523 Stress. *ACS Chemical Biology*, *15*(9), 2558–2567.
524 <https://doi.org/10.1021/acscchembio.0c00591>

525 Jakobek, L., & Matic, P. (2019). Non-covalent dietary fiber - Polyphenol interactions
526 and their influence on polyphenol bioaccessibility. *Trends in Food Science and*
527 *Technology*, *83*, 235–247. <https://doi.org/10.1016/j.tifs.2018.11.024>

528 Koch, W. (2019). Dietary polyphenols-important non-nutrients in the prevention of
529 chronic noncommunicable diseases. A systematic review. *Nutrients*, *11*(5), 1–35.
530 <https://doi.org/10.3390/nu11051039>

531 Le Bourvellec, C., Boas, P. B. V., Lepercq, P., Comtet-Marre, S., Auffret, P., Ruiz,
532 P., ... Mosoni, P. (2019). Procyanidin—cell wall interactions within apple
533 matrices decrease the metabolization of procyanidins by the human gut
534 microbiota and the anti-inflammatory effect of the resulting microbial
535 metabolome in vitro. *Nutrients*, *11*(3), 664. <https://doi.org/10.3390/nu11030664>

536 Le Bourvellec, C., Bouchet, B., & Renard, C. M. G. C. (2005). Non-covalent
537 interaction between procyanidins and apple cell wall material. Part III: Study on
538 model polysaccharides. *Biochimica et Biophysica Acta - General Subjects*,
539 *1725*(1), 10–18. <https://doi.org/10.1016/j.bbagen.2005.06.004>

540 Le Bourvellec, C., Watrelot, A. A., Ginies, C., Imbert, A., & Renard, C. M. G. C.
541 (2012). Impact of processing on the noncovalent interactions between
542 procyanidin and apple cell wall. *Journal of Agricultural and Food Chemistry*,
543 *60*(37), 9484–9494. <https://doi.org/10.1021/jf3015975>

544 Liu, X., Le Bourvellec, C., Guyot, S., & Renard, C. M. G. C. (2021). Reactivity of
545 flavanols: Their fate in physical food processing and recent advances in their
546 analysis by depolymerization. *Comprehensive Reviews in Food Science and*
547 *Food Safety*, 1–40. <https://doi.org/10.1111/1541-4337.12797>

548 Liu, X., Le Bourvellec, C., & Renard, C. M. G. C. (2020). Interactions between cell
549 wall polysaccharides and polyphenols: Effect of molecular internal structure.

550 *Comprehensive Reviews in Food Science and Food Safety*, 19(6), 3574–3617.
551 <https://doi.org/10.1111/1541-4337.12632>

552 Liu, X., Renard, C. M. G. C., Bureau, S., & Le Bourvellec, C. (2021). Interactions
553 between heterogeneous cell walls and two procyanidins: Insights from the effects
554 of chemical composition and physical structure. *Food Hydrocolloids*, 121,
555 107018. <https://doi.org/10.1016/j.foodhyd.2021.107018>

556 Liu, X., Renard, C. M. G. C., Rolland-Sabaté, A., Bureau, S., & Le Bourvellec, C.
557 (2021). Modification of apple, beet and kiwifruit cell walls by boiling in acid
558 conditions: Common and specific responses. *Food Hydrocolloids*, 112, 106266.
559 <https://doi.org/10.1016/j.foodhyd.2020.106266>

560 Liu, X., Renard, C. M. G. C., Rolland-Sabaté, A., & Le Bourvellec, C. (2021).
561 Exploring interactions between pectins and procyanidins: Structure-function
562 relationships. *Food Hydrocolloids*, 113, 106498.
563 <https://doi.org/10.1016/j.foodhyd.2020.106498>

564 Lu, T., & Chen, F. (2012). Multiwfn: A multifunctional wavefunction analyzer.
565 *Journal of Computational Chemistry*, 33(5), 580–592.
566 <https://doi.org/10.1002/jcc.22885>

567 Murray, J. S., & Politzer, P. (2011). The electrostatic potential: An overview. *Wiley*
568 *Interdisciplinary Reviews: Computational Molecular Science*, 1(2), 153–163.
569 <https://doi.org/10.1002/wcms.19>

570 Pérez, S., & Rivet, A. (2021). Polys Glycan Builder: An online application for
571 intuitive construction of 3D structures of complex carbohydrates, in methods in
572 molecular biology. In T. Lutteke (Ed.), *Glycoinformatics: Methods and protocols*
573 (Second Edi).

574 Pérez, S., Tubiana, T., Imbert, A., & Baaden, M. (2015). Three-dimensional
575 representations of complex carbohydrates and polysaccharides - SweetUnityMol:
576 A video game-based computer graphic software. *Glycobiology*, 25(5), 483–491.
577 <https://doi.org/10.1093/glycob/cwu133>

578 Phan, A. D. T., Flanagan, B. M., D'Arcy, B. R., & Gidley, M. J. (2017). Binding

579 selectivity of dietary polyphenols to different plant cell wall components:
580 Quantification and mechanism. *Food Chemistry*, 233, 216–227.
581 <https://doi.org/10.1016/j.foodchem.2017.04.115>

582 Poncet-Legrand, C., Gautier, C., Cheynier, V., & Imberty, A. (2007). Interactions
583 between flavan-3-ols and poly(L-proline) studied by isothermal titration
584 calorimetry: Effect of the tannin structure. *Journal of Agricultural and Food*
585 *Chemistry*, 55(22), 9235–9240. <https://doi.org/10.1021/jf071297o>

586 Pracht, P., Bohle, F., & Grimme, S. (2020). Automated exploration of the low-energy
587 chemical space with fast quantum chemical methods. *Physical Chemistry*
588 *Chemical Physics*, 22(14), 7169–7192. <https://doi.org/10.1039/c9cp06869d>

589 Renard, C. M. G. C., Watrelot, A. A., & Le Bourvellec, C. (2017). Interactions
590 between polyphenols and polysaccharides: Mechanisms and consequences in
591 food processing and digestion. *Trends in Food Science and Technology*, 60, 43–
592 51. <https://doi.org/10.1016/j.tifs.2016.10.022>

593 Rolland-Sabaté, A., Colonna, P., Potocki-Véronèse, G., Monsan, P., & Planchot, V.
594 (2004). Elongation and insolubilisation of α -glucans by the action of *Neisseria*
595 *polysaccharea* amylosucrase. *Journal of Cereal Science*, 40(1), 17–30.
596 <https://doi.org/10.1016/j.jcs.2004.04.001>

597 Ruiz-Garcia, Y., Smith, P. A., & Bindon, K. A. (2014). Selective extraction of
598 polysaccharide affects the adsorption of proanthocyanidin by grape cell walls.
599 *Carbohydrate Polymers*, 114, 102–114.
600 <https://doi.org/10.1016/j.carbpol.2014.07.024>

601 Saura-Calixto, F., & Pérez-Jiménez, J. (2018). *Non-extractable Polyphenols and*
602 *Carotenoids*. (F. Saura-Calixto & J. Pérez-Jiménez, Eds.) (Vol. 5). Royal Society
603 of Chemistry. <https://doi.org/doi.org/10.1039/9781788013208>

604 Seal, C. J., Courtin, C. M., Venema, K., & de Vries, J. (2021). Health benefits of
605 whole grain: effects on dietary carbohydrate quality, the gut microbiome, and
606 consequences of processing. *Comprehensive Reviews in Food Science and Food*
607 *Safety*. <https://doi.org/10.1111/1541-4337.12728>

608 Selig, M. J., Thygesen, L. G., Felby, C., & Master, E. R. (2015). Debranching of
609 soluble wheat arabinoxylan dramatically enhances recalcitrant binding to
610 cellulose. *Biotechnology Letters*, 37(3), 633–641.
611 <https://doi.org/10.1007/s10529-014-1705-0>

612 Shrestha, U. R., Smith, S., Pingali, S. V., Yang, H., Zahran, M., Breunig, L., ...
613 Petridis, L. (2019). Arabinose substitution effect on xylan rigidity and
614 self-aggregation. *Cellulose*, 26(4), 2267–2278.
615 <https://doi.org/10.1007/s10570-018-2202-8>

616 Turnbull, W. B., & Daranas, A. H. (2003). On the value of c: Can low affinity
617 systems be studied by isothermal titration calorimetry? *Journal of the American*
618 *Chemical Society*, 125(48), 14859–14866. <https://doi.org/10.1021/ja036166s>

619 Waskom, M. (2014). Seaborn: Statistical Data Visualization. Retrieved from
620 <http://stanford.edu/~mwaskom/software/seaborn/>

621 Watrelot, A. A., Le Bourvellec, C., Imbert, A., & Renard, C. M. G. C. (2013).
622 Interactions between pectic compounds and procyanidins are influenced by
623 methylation degree and chain length. *Biomacromolecules*, 14(3), 709–718.
624 <https://doi.org/10.1021/bm301796y>

625 Watrelot, A. A., Le Bourvellec, C., Imbert, A., & Renard, C. M. G. C. (2014).
626 Neutral sugar side chains of pectins limit interactions with procyanidins.
627 *Carbohydrate Polymers*, 99, 527–536.
628 <https://doi.org/10.1016/j.carbpol.2013.08.094>

629
630
631